ACS NANO
Cite This: ACS Nano XXXX, XXX, XXX-XXX
www.acsnano.org

ARTICLE

Hydrothermally Activated Graphene Fiber Fabrics for Textile Electrodes of Supercapacitors

Zheng Li, Tieqi Huang, Weiwei Gao,* Zhen Xu, Dan Chang, Chunxiao Zhang, and Chao Gao*

MOE Key Laboratory of Macromolecular Synthesis and Functionalization, Department of Polymer Science and Engineering, Key Laboratory of Adsorption and Separation Materials & Technologies of Zhejiang Province, Zhejiang University, 38 Zheda Road, Hangzhou 310027, China

Supporting Information

ABSTRACT: **Carbon textiles are promising electrode materials for wearable energy storage devices owing to their conductive, flexible, and lightweight features. However, there still lacks a perfect choice for high-performance carbon textile electrodes with sufficient electrochemical activity. Graphene fiber fabrics (GFFs) are newly discovered carbon textiles, exhibiting various attractive properties, especially a large variability on the microstructure. Here we report the fabrication of hierarchical GFFs with significantly enlarged specific surface area using a hydrothermal activation strategy. By carefully optimize the activation process, the hydrothermally activated graphene fiber fabrics (HAGFFs) could achieve an areal capacitance of 1060 mF cm^{-2} in a very thin thickness (150 μm) and the capacitance is easily magnified by overlaying several layers of HAGFFs, even up to a record value of 7398 mF cm^{-2}. Meanwhile, a good rate capability and a long cycle life are also attained. As compared with other carbon textiles, including the commercial carbon fiber cloths, our HAGFFs present much better capacitive performance. Therefore, the mechanically stable, flexible, conductive, and highly active HAGFFs have provided an option for high-performance textile electrodes.**

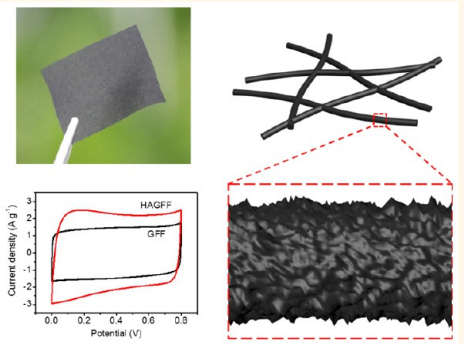

KEYWORDS: *graphene fiber fabrics, supercapacitors, textile electrodes, hydrothermal activation, hierarchical structure, areal capacitance*

Carbon textiles are of great promise as electrodes in wearable energy storage devices because of their high conductivity and flexibility, network structure, low cost, and a lightweight attribute.[1−3] Supercapacitors are characterized with high power density, fast charge/discharge rate, and long lifetime as well as a less complex configuration as compared with batteries.[4−6] The application of carbon textiles in supercapacitors has been intensively studied.[2,3,7,8]

Typically, the state-of-the-art carbon textile electrodes could be divided into three categories: (1) carbon coated textiles obtained by conformal coating carbon materials (CNTs, graphene, *etc.*) on flexible yet isolating substrates such as cellulose papers, cotton fabrics, polymeric wovens/nonwovens, and so on;[9−14] (2) carbonized textiles originating from cotton or polymeric mats/cloths;[15−19] and (3) commercial carbon fiber cloths and their activated forms.[20−23] Although they are at low cost, the present carbon textiles have their own disadvantages. For the carbon-coated textiles, the non-electroactive substrates seriously undermine the overall performance of the hybrid electrodes, while the detachment of active carbons is a typical issue that degrades the durability and cycle life of the electrodes. The carbonized textiles usually suffer from poor mechanical stability of the textile structure. Currently, the commercial carbon fiber cloths are the most popular carbon textile electrodes because of their good mechanical and conductive properties. However, their capacitive performance is relatively low, in term of limited specific capacitances, which is mainly attributed to the poor electrochemical activity of carbon fibers. Up to now, the discovery of high-performance carbon textile electrodes with sufficient electrochemical activity is still challenging.

The nonwoven graphene fiber fabric (GFF), reported by our group recently, is a new member of the big family of carbon textiles. With a network structure of interfused graphene fibers, the GFFs are flexible, robust, and highly conductive.[24] Since graphene fibers have attracted extensive attention as perfect fiber electrodes for wearable supercapacitors,[25−31] the GFFs could offer a potential choice for high-performance textile electrodes. In addition, the characteristics of 2D graphene

Received: July 19, 2017
Accepted: October 16, 2017
Published: October 16, 2017

DOI: 10.1021/acsnano.7b05092
ACS Nano XXXX, XXX, XXX−XXX

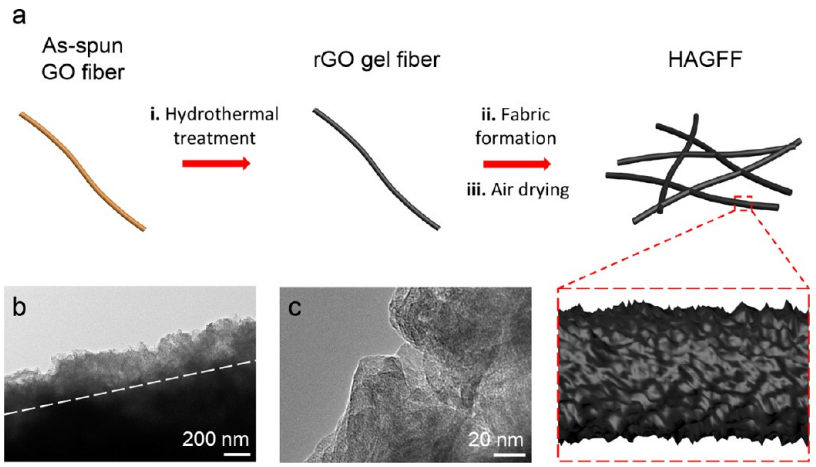

Figure 1. (a) Schematic illustration of the hydrothermal activation process for HAGFF with a hierarchical structure. TEM images focused at the edge of the hierarchical fiber within HAGFF at (b) low and (c) high magnification.

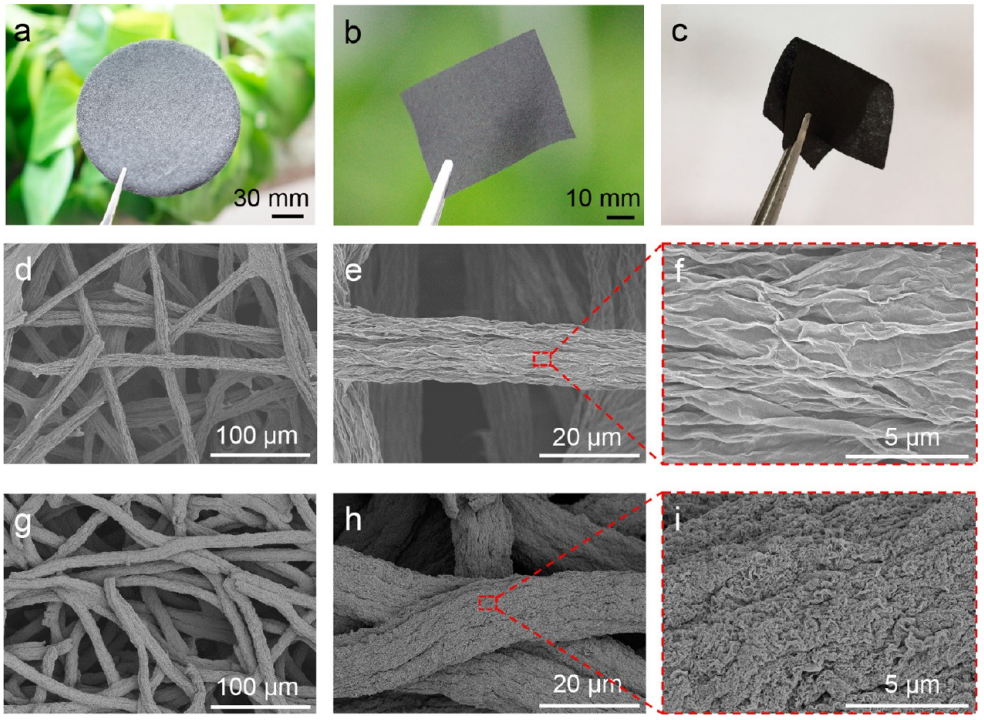

Figure 2. Photographs of (a) regular GOFF, (b) HAGFF, and (c) HAGFF in the bending state. SEM images of (d–f) GOFF and (g–i) HAGFF under different magnifications.

sheets provide possibilities for easy control on the microstructure of GFFs, facilitating a further activation procedure for enhanced electrochemical activity.

One direct way for activating carbon textiles is to increase their specific surface area (SSA).[21,22,32] Here, through a hydrothermal activation strategy, we fabricated electrochemically active GFFs with a hierarchical morphology. In such a process, crumpling of the graphene sheets within graphene fibers made for efficient activation on GFFs with largely increased SSA. Meanwhile, the microstructure of the activated GFFs could be precisely controlled by adjusting the activation conditions. As a result, a single layer (150 μm) of hydrothermally activated GFF (HAGFF) showed a maximum areal capacitance (an important parameter for evaluation of textile electrodes in practice) of 1060 mF cm^{-2}, which is more than 3 times higher than that of the untreated regular GFFs, and significantly outperforms previous carbon textile electrodes. Besides, a good rate capability, a long cycle life (50000 charge/discharge cycles), as well as an energy density of 23.5 μWh cm^{-2} and a power density of 26.3 mW cm^{-2} were also achieved. Moreover, an areal capacitance as high as 7398 mF cm^{-2} was attained by stacking 5 layers of the HAGFFs (5 × 200 μm). The structural durability of the HAGFF electrodes was also demonstrated in a flexible all-solid-state supercapacitor. In combination with mechanical stability, flexibility, conductivity, and electrochemical activity, our HAGFFs make a promising candidate for high-performance textile electrodes.

RESULTS AND DISCUSSION

Our fabrication and activation procedure for HAGFFs is illustrated in Figure 1a, including three main steps: (i) the wet-spun GO fibers after fully dried at a mild temperature were

DOI: 10.1021/acsnano.7b05092
ACS Nano XXXX, XXX, XXX–XXX

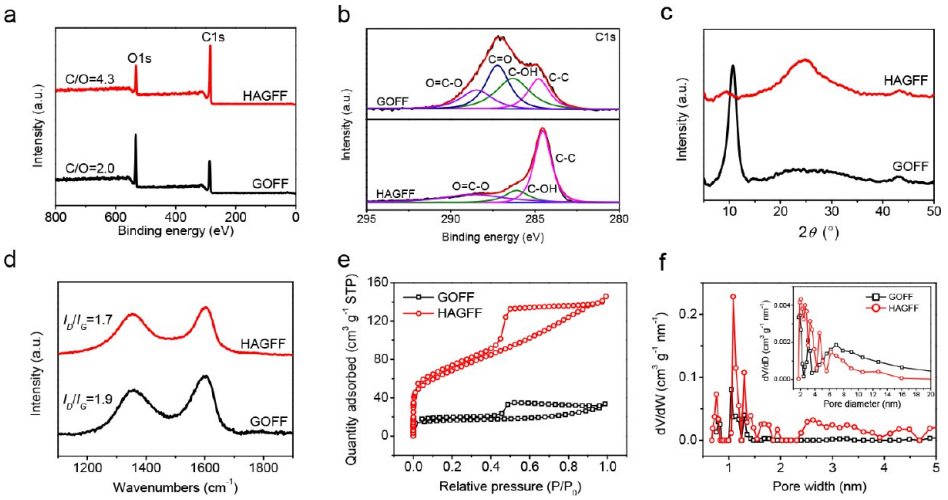

Figure 3. Characterization of regular GOFF and HAGFF: (a) XPS spectra, (b) C 1s spectra, (c) XRD patterns, (d) Raman spectra, (e) nitrogen adsorption isotherms collected at 77 K, and (f) pore size distribution.

taken to hydrothermal treatment for 10 h; (ii) the partially reduced GO (rGO) gel fibers were then cut into microfiber staples *via* high-speed shearing in water, followed by a filtration process to form a nonwoven fabric; (iii) the wet product was finally air-dried allowing for the formation of the HAGFFs with hierarchical morphology, in term of highly wrinkled microstructures. As evidenced by the transmission electron microscopy (TEM) images (Figure 1b,c), the constituent graphene fibers after hydrothermal activation are formed by stacking the crumpled graphene sheets. The thickness of the rough shell is about 300 nm as indicated in Figure 1b. For comparison, we made regular GOFFs (GO fiber fabrics before reduction) and GFFs (reduced GOFFs) as control samples, following a similar procedure for HAGFF, but without hydrothermal treatment before fabric formation (see details in the experimental section).

It is worth mentioning that although we mainly focused on the final product of HAGFFs in the current study, the hydrothermal activation strategy is primarily an efficient approach for acquiring hierarchical graphene fibers from ordinary ones. On the basis of the well-established continuous wet-spinning technique,[33,34] our strategy is more readily scalable as compared with the previous dimensionally confined hydrothermal strategy,[35] as the latter is performed on a limited amount of GO suspension, rather than massive as-spun GO fibers. Actually, the fabrication of GFFs relies heavily on such a large-scale production capacity.

Since the hydrothermal process is known to reduce GO materials,[36−38] the change of appearance from dark brown (GOFF) to black (HAGFF) is indicative of the reduction of GO fibers (Figure 2a,b). Figure 2c shows that the resultant HAGFF is flexible enough to be bent to 180°, originating from its stable fabric construction, as well as the flexibility of the activated graphene fibers. A textile feature (an open framework that is permeable to light) is also seen in Figure 2c. The scanning electron microscopy (SEM) images (Figure 2d−i) present the difference between GOFF and HAGFF in their microstructure. Evidently, the rGO fibers in HAGFF exhibit massive wrinkled microstructures spreading on the fiber surface (Figure 2g−i). By contrast, the fibers in GOFF are of much lower roughness (Figure 2d−f). Therefore, the HAGFF is proven to have a hierarchical morphology after hydrothermal activation; meanwhile, its flexibility is retained. More specifically, the structural hierarchy of HAGFF could be divided into three levels from the macro- to the nanoscale: fiber network with large open pores, randomly oriented graphene fibers, and fine wrinkled substructures on the surface and within the fibers.

The X-ray photoelectron spectroscopy (XPS) survey (Figure 3a) certifies the hydrothermal reduction on HAGFF, evidenced by the increased C/O ratio as compared with that of the regular GOFF (from 2.0 of GOFF to 4.3 of HAGFF). Detailed elemental analysis of C and O content is provided in Table S1. The comparison of the high resolution C 1s and O 1s spectra indicate the significant loss of functional groups in HAGFF. As shown in Figure 3b, the C 1s spectra were deconvoluted into four peaks, corresponding to C−C (284.8 eV), C−O (286.3 eV), C═O (287.2 eV), and O−C═O (288.5 eV), respectively. After hydrothermal treatment, the content of the oxygen-containing functional groups reduced sharply and the C═O groups were barely seen in the spectra of HAGFF. Similarly, the O 1s spectra of HAGFF also reveal a weakened signal relative to the GOFF (Figure S1), which can be deconvoluted into two groups: singly bonded oxygen (533.0 eV) and doubly bonded oxygen (531.5 eV).[39,40] Figure 3c shows the X-ray diffraction (XRD) patterns of GOFF and HAGFF. According with the XPS results, the characteristic peak of GOFF at about 10.7° (corresponding to an interlayer spacing of 8.6 Å) is attributed to the existence of a large amount of oxidative groups, which are mostly eliminated in HAGFF, revealed by the absence of such a sharp peak. The restacking of rGO sheets caused by reduction led to the appearance of the (002) diffraction peak (~24.5°, *d*-spacing = 3.7 Å), the broad span is indicative of a disordered stacking resulting from the highly wrinkled graphene sheets. In addition, an inconspicuous difference is seen in Raman spectra between GOFF and HAGFF, but a slight decrease of the D:G peak intensity ratio from 1.9 to 1.7 is found (Figure 3d). Distinct from the destructive activation on carbon fibers,[22] in our case, Raman results reveal that the sp2 structure of graphene sheets is partially recovered *via* hydrothermal treatment, which is consistent with some other references.[36,41,42] The N_2 adsorption−desorption isotherms and pore size distribution of GOFF and HAGFF are shown in Figure 3 panels e and f. Both the GOFF and HAGFF exhibit Type IV

DOI: 10.1021/acsnano.7b05092
ACS Nano XXXX, XXX, XXX−XXX

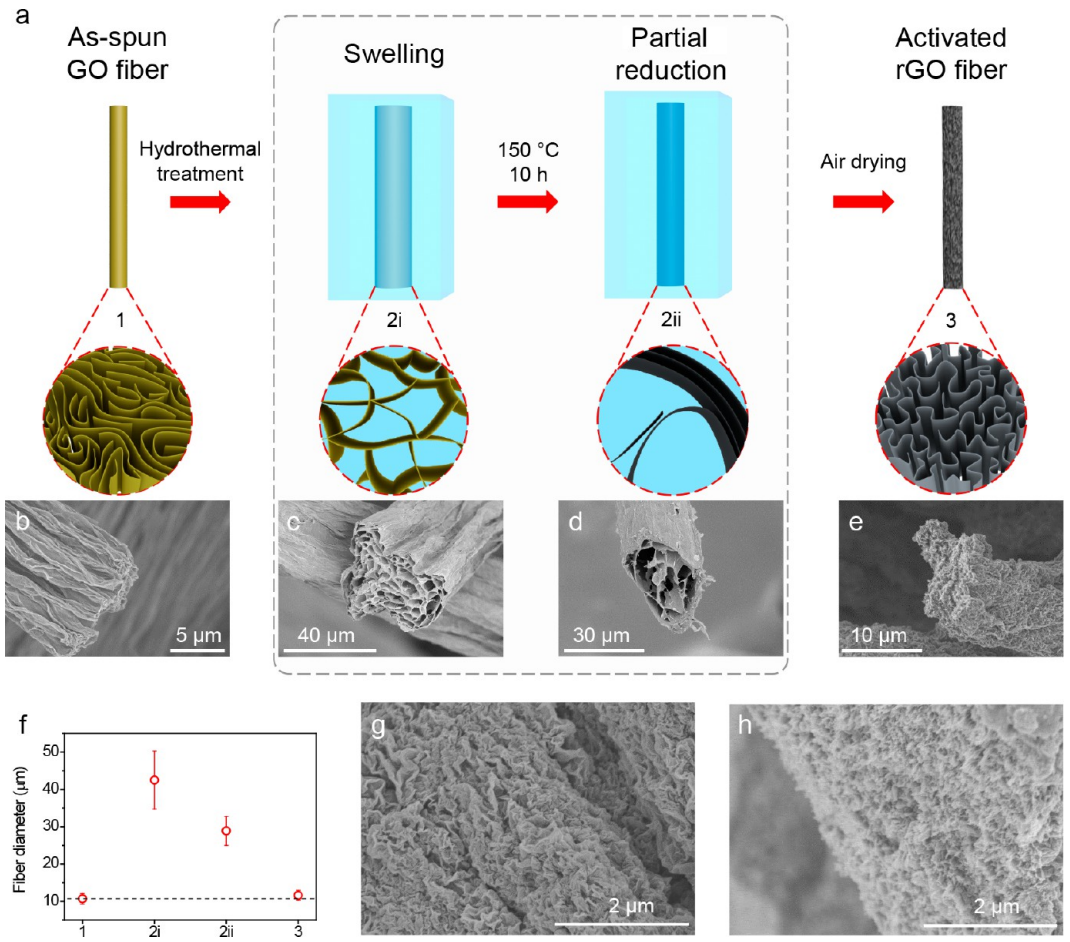

Figure 4. (a) Schematic diagram showing the structural evolution of graphene fibers during the hydrothermal activation process. Cross-sectional SEM images of graphene fibers in the corresponding stages: (b) as-spun GO fiber (1); (c) swelled GO gel fiber at the beginning of hydrothermal treatment (2i); (d) rGO gel fiber at the end of hydrothermal treatment (2ii), and (e) the resulted hierarchical rGO fiber after air-drying (3); (f) variation of the fiber diameter during hydrothermal activation; (g) surface and (h) sectional topography of activated graphene fibers at high magnification.

adsorption (Figure 3e). The Brunauer–Emmett–Teller (BET) surface area of GOFF is 52 $m^2 g^{-1}$, while the SSA of HAGFF is significantly increased to 245 $m^2 g^{-1}$ (about 370% higher) upon hydrothermal activation. The steep uptake at low relative pressure (P/P_0 < 0.1) in the N_2 adsorption–desorption isotherms is indicative of a large number of micropores (<2 nm) within the fibers, and the hysteresis loop located at 0.4 < P/P_0 < 1 suggests the presence of mesopores (2–50 nm),[43,44] which are both more abundant in the activated HAGFF. Additionally, the pore size distribution was calculated by the nonlocal density function theory (NLDFT) method for micropores and the Barrett–Joyner–Halenda (BJH) method for mesopores.[15] It confirms that most of the pore structures fall in the range below 10 nm (Figure 3f). The BET results are in accordance with the morphological observation. They collectively demonstrate that the hierarchical morphology induced by hydrothermal activation has led to a considerably larger surface area and pore volume in the HAGFF, which may enhance the activity of GFFs in their electrode applications.

Former studies indicated that hydrothermally treated GO aqueous solution would give rise to a high density monolith after ambient drying.[35,41,45–47] However, hydrothermal treatment on solid graphene assemblies, as being an activation protocol for as-formed fibers/films/fabrics, was never reported. More significantly, we believe it could become a general activation strategy for various densely packed GO-based assemblies, through inducing wrinkled substructures therein. Regarding this, comprehensive understanding of the structural evolution of graphene fibers during the hydrothermal activation process is critical for precise control on the resultant hierarchical morphology.

In Figure 4a, we proposed a mechanism for the formation of hierarchical fiber structure *via* hydrothermal activation, which is technically applicable to many GO-based assemblies, as long as the hydrophilicity of the GO sheets is well-preserved. Generally, the structural evolution could be divided into four stages: (1) first, GO fibers were spun and predried exhibiting a compact and lamellar morphology in the cross section (Figure 4b). (2i) While the fibers were taken to hydrothermal treatment, the hydrophilic fibers should swell quickly as soon as their contact with water. The freeze-dried GO fibers in stage 2i showed apparently expanded fiber diameter (from ~10.7 μm to ~42.5 μm, Figure 4f) and highly porous inner-fiber structure, indicative of a thorough swelling (Figure 4c) in the initial stage of the hydrothermal process. (2ii) After being heated at 150 °C for 10 h, the fibers were partially reduced and shrunk to a certain extent (~28.9 μm) (Figure 4d,f), because of the decreased electrostatic repulsion and enhanced hydrophobic interaction among rGO sheets due to hydrothermal reduction. (3) Finally, the drying process in ambient condition generated

DOI: 10.1021/acsnano.7b05092
ACS Nano XXXX, XXX, XXX–XXX

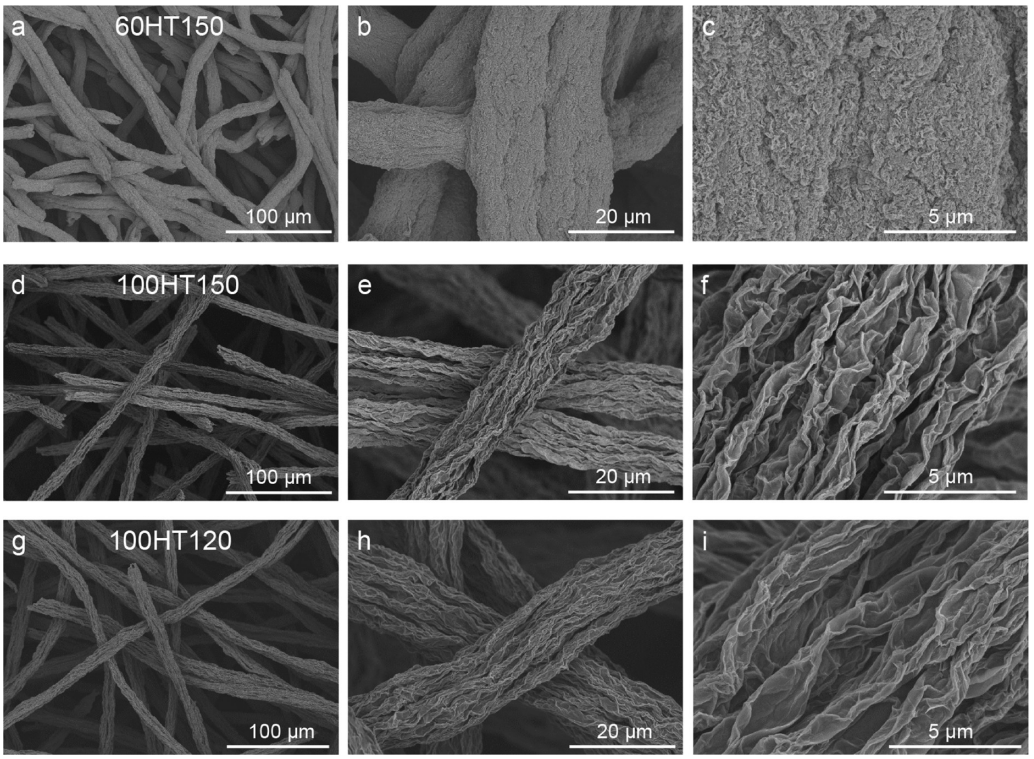

Figure 5. Effects of predrying and hydrothermal treatment conditions on the morphology of the resulting HAGFFs. SEM images of activated GFFs under different treatment conditions: (a–c) 60HT150, 60 °C predried and 150 °C hydrothermally treated; (d–f) 100HT150, 100 °C predried and 150 °C hydrothermally treated; and (g–i) 100HT120, 100 °C predried and 120 °C hydrothermally treated.

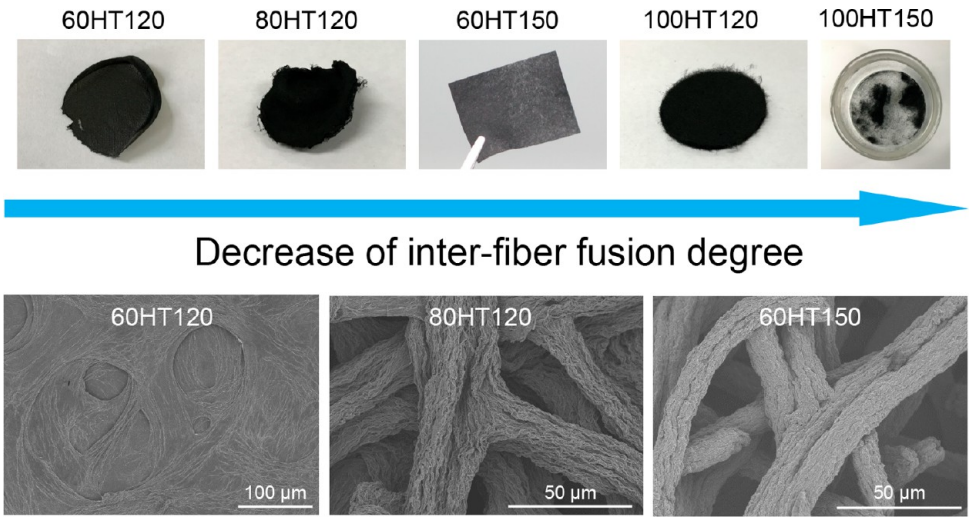

Figure 6. Variation of interfiber fusion degree in different activating conditions. Upper row: photos of the products obtained in the indicated conditions. Bottom row: SEM images showing the over fusion in 60HT120 and fused junctions in 80HT120 and 60HT150.

tremendous wrinkles on the rGO sheets and resulted in the hierarchical morphology (Figure 4e), which is similar to that in the literature which reports the fabrication of high density graphene monoliths,[41,45,46] and the crumpling of rGO sheets is thought to be originated from the thermally generated strain on graphene sheets.[48] Different from the as-spun fibers possessing a nearly face-to-face stacking of flat GO sheets, the corrugation of rGO sheets may lead to higher roughness on the fiber surface (Figure 4g) and larger pore volume inside the fiber (Figure 4h); both contribute to the increased SSA. In the meantime, the close stacking of the crumpled rGO sheets, reflected by the slightly increased fiber diameter (Figure 4f and Figure S2), ensures a certain conductivity within the fiber.

By taking full advantage of their swelling behavior, the compact GO assemblies could be hydrothermally activated. Therefore, the predrying (affecting the hydrophilicity of GO) and hydrothermal treatment are two key processes determining the geometry of the final products. In our current study, the temperature for the two processes is carefully optimized. We chose 60–100 °C for predrying and 120–150 °C for hydrothermal treatment. The corresponding HAGFFs are denoted as *x*HT*y*, where *x* indicates the predrying temperature and *y* indicates the hydrothermal treatment temperature,

DOI: 10.1021/acsnano.7b05092
ACS Nano XXXX, XXX, XXX–XXX

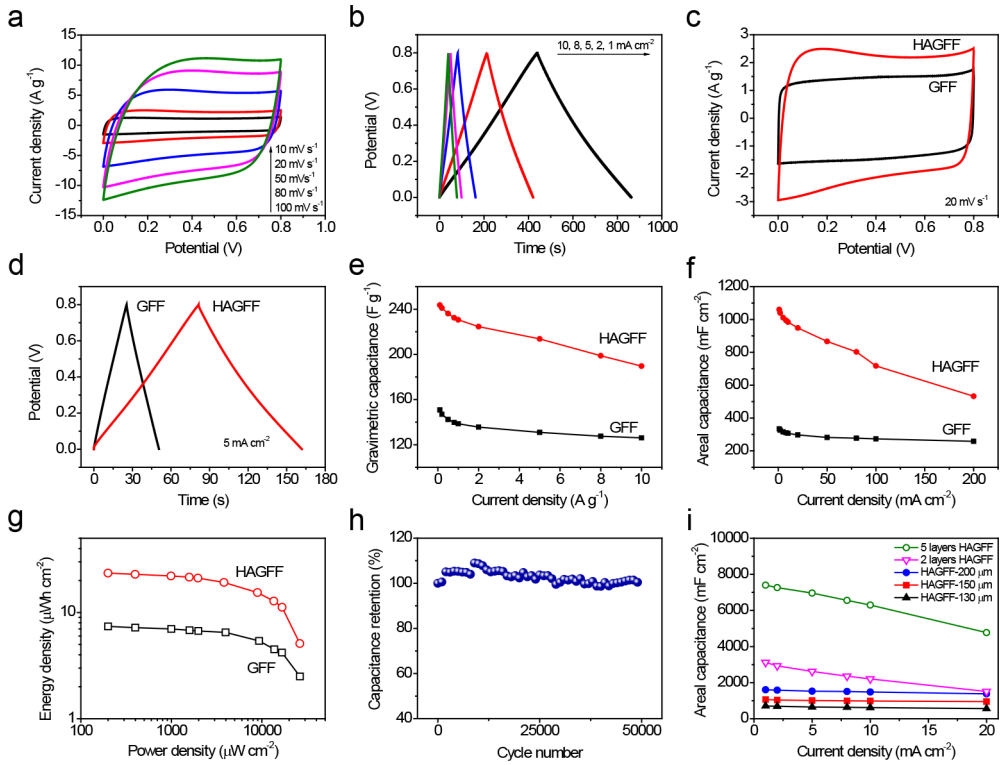

Figure 7. Electrochemical performance of the HAGFF electrodes as compared to that of the GFF electrodes: (a) CV curves of HAGFF at scan rates from 10 to 100 mV s^{-1}; (b) GCD curves of HAGFF at charging/discharging current densities from 1 to 10 mA cm^{-2}; (c) comparison of the CV curves of HAGFF and GFF collected at 20 mV s^{-1}; (d) single cycle of GCD curves at 5 mA cm^{-2} for HAGFF and GFF; (e) calculated C_G of HAGFF and GFF; (f) C_A of HAGFF and GFF; (g) Ragone plots of HAGFF and GFF electrodes based supercapacitors; (h) cycling behavior of HAGFF at 1 A g^{-1} for 50000 cycles; (i) C_A of HAGFF electrodes with various thicknesses.

respectively. Generally, a higher predrying temperature may reduce the swelling degree of the GO fiber (Figure S3), and thus has negative effect on the activation, evidenced by the weakened wrinkling in 100HT150 as compared with 60HT150 (Figure 5a–f). On the other hand, hydrothermal treatment at lower temperature will also generate less crumples, as reflected in 100HT120 (Figure 5g–i).

As discussed in our previous work, the interfusion between graphene fibers is the key to realize high-performance GFFs.[24] For the fabrication of HAGFFs, a proper interfiber fusion should also be taken into consideration, since the fused junctions guarantee the structural stability and conductivity of the fabrics. The fusion degree between fibers could be readily controlled by adjusting the two critical temperatures. When the predrying temperature increases, the interfusion between fibers is impeded, and the increase of hydrothermal treating temperature shows the same trend (Figure 6). There are two extreme cases: (1) fibers in 60HT120 were overfused which led to the miss of a network structure, and got a less porous paper-like product; (2) fibers in 100HT150 were completely not fused and thus failed to obtain a fabric. In 80HT120 and 60HT150, the activated fibers were appropriately interfused. More details are shown in Figure S4. In overall consideration of the microstructure and interfiber fusion of the activated fibers, the optimum conditions for HAGFFs were set as 60 °C predrying and 150 °C hydrothermal treatment. Thus, the mechanically stable, flexible, and electrochemically active HAGFFs could be realized.

Benefiting from the well-constructed hierarchical structure, the activated fabrics with increased SSA are promising for electrodes in electrochemical double-layer capacitors (EDLCs). The HAGFFs were further reduced by hydrazine hydrate (N_2H_4) to improve the conductivity, achieving a better value (~4 S m^{-1}) than that of the activated carbon fiber cloths reported in the literature.[49] XRD, Raman, and XPS spectra of the N_2H_4 reduced HAGFFs are shown in Figure S5.

The electrochemical performance of HAGFF was investigated in a conventional two-electrode system, with 1 M H_2SO_4 as the aqueous electrolyte solution. The cyclic voltammetry (CV) curves of HAGFF electrodes at various scan rates from 10 to 100 mV s^{-1} are presented in Figure 7a, showing a nearly rectangular shape with good symmetry. Meanwhile, the shape of CV curves is maintained at high scan rates even up to 100 mV s^{-1}, indicating a good conductivity of the EDLC electrodes. The galvanostatic charge–discharge (GCD) curves of HAGFF acquired at current densities ranging from 1 to 10 mA cm^{-2} exhibit a symmetrical profile, as well as insignificant IR drop (only 0.0013 V at 10 mA cm^{-2}), also representing an extremely low internal resistance in the EDLC system (Figure 7b). Figure 7c shows the comparison of CV curves of HAGFF and GFF collected at 20 mV s^{-1}. The enclosed area is visibly larger in the CV curve of HAGFF, demonstrating a better energy storage ability for the activated hierarchical fabrics. The GCD curves further confirm the superior capacitive performance of HAGFF electrodes by the substantially prolonged discharge time (Figure 7d). The calculated gravimetric and areal capacitance provided quantitative evidence of better capacitive behavior in HAGFF. The specific capacitance values of HAGFF are all above those of GFF. The specific gravimetric capacitance (C_G) of HAGFF reaches a value of 244 F g^{-1} at a current density of 0.1 A g^{-1} (Figure 7e). Notably, the specific areal capacitance (C_A) of

DOI: 10.1021/acsnano.7b05092
ACS Nano XXXX, XXX, XXX–XXX

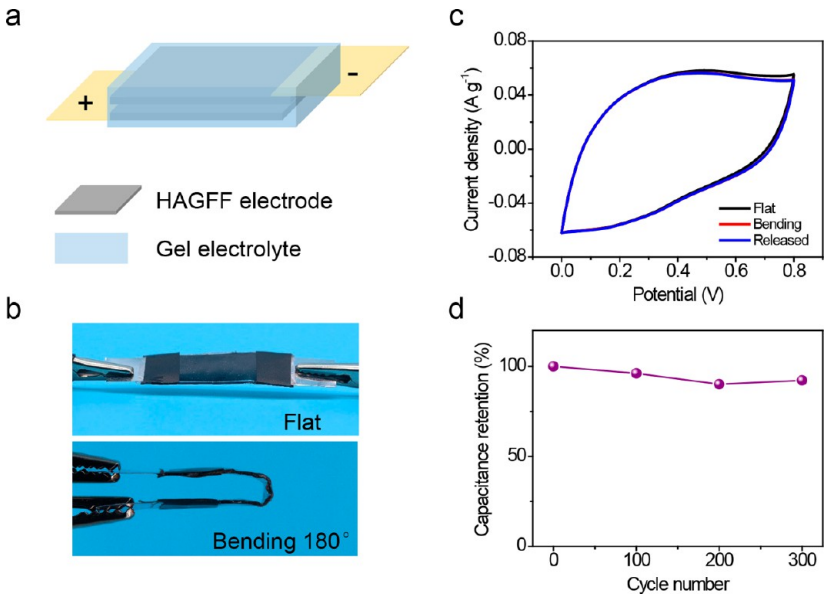

Figure 8. (a) Schematic diagram illustrating the architecture of an all-solid-state supercapacitor based on HAGFF electrodes and PVA/H_2SO_4 gel electrolyte; (b) photographs of the flexible supercapacitor at flat (top) and 180° bending (bottom) state, respectively; (c) comparison of CV curves at 2 mV s^{-1} of the flexible supercapacitor at a flat state, bending at 180°, and released from bending; (d) capacitance retention of the solid-state supercapacitor after up to 300 bending cycles.

HAGFF (1060 mF cm^{-2} at 1 mA cm^{-2}) is higher than most of the carbon textile electrodes (Figure 7f). By the way, the calculation of C_A is normally on the basis of the geometric area of the electrodes, since such a capacitance value is of practical meaning for their application in wearable devices, as is normally done by others.[2] For regular GFF, its C_A of 334 mF cm^{-2} is three times lower than that of HAGFF. The specific capacitance of HAGFF decreases with increasing current density, but still, it shows good rate performance with retention of 84% and 68% for C_G and C_A, respectively, while the current densities increase to 100 times higher (from 0.1 A g^{-1} to 10 A g^{-1} for C_G and from 1 mA cm^{-2} to 100 mA cm^{-2} for C_A). Ragone plots of energy density versus power density for the symmetric supercapacitors based on HAGFF and GFF are provided in Figure 7g. Clearly with higher performance than the GFF based supercapacitor, the HAGFF based one has the maximum areal energy density (E_A) of 23.5 μWh cm^{-2} at a current density of 1 mA cm^{-2}, while its areal power density (P_A) could reach 26.3 mW cm^{-2} when the current density increases to 200 mA cm^{-2}, much better than those of previously reported textile-based supercapacitors.[10,11] The gravimetric and volumetric energy density and power density of the HAGFF-based device are also presented in the Supporting Information (Figure S6), showing higher values than those achieved in the supercapacitors assembled with activated carbon fiber cloth electrodes.[21,22] Electrochemical impedance spectroscopy (EIS) shown in Figure S7 is helpful for investigating the electrochemical process. The nearly vertical curves in the low-frequency region are indicative of ideal capacitive behavior in both GFF and HAGFF. The followed 45° Warburg region corresponds to the ion diffusion from electrolyte into the electrode. In the high-frequency region, the semicircle displayed in the plots represents the interfacial charge transfer resistance (R_{ct}), which was calculated as ~0.7 Ω and ~2.5 Ω for GFF and HAGFF, respectively. The increased R_{ct}, showing relatively difficult ion diffusion and transfer in the HAGFF-based capacitor, is attributed to the abundant micro- and mesopores in HAGFF derived by activation.[22,50] The HAGFF electrodes have a long cycle life with no capacitance decay after 50000 cycles, as shown in Figure 7h. The above results reveal that the hydrothermally activated HAGFFs with hierarchical configuration have shown dramatically improved capacitive performance.

Generally for textile electrodes, the open pores within the textiles not only endow the electrodes with flexibility and lightweight, but also provide free pathways for ion transport during the electrochemical process. Meanwhile, the conductive scaffolds constructed by fibrous materials are capable of facilitating fast electron conduction. Through hydrothermal activation on graphene fibers, the increased roughness and porosity contribute an enlarged active surface area to the resulted HAGFFs. Besides, the residual oxygenated functionalities in the electrodes after N_2H_4 reduction should provide a certain amount of pseudocapacitance during the measurement, leading to a higher overall capacitance.[6,51] As compared with a previous work on carbon textile electrodes, our HAGFFs composed of hierarchical graphene fibers exhibit the highest capacitance values (Table S2).

We also noticed that the C_A could be evidently improved by increasing the thickness of electrodes, owing to the increased active mass per unit area.[23,49] As shown in Figure 7i, the maximum capacitance of HAGFF raises linearly from 706 mF cm^{-2} to 1607 mF cm^{-2} while its thickness increases from 130 to 200 μm. However, the C_G does not follow the same trend (Figure S8), which gets to a peak value of 244 F g^{-1} for a 150 μm thick electrode and then drops to 168 F g^{-1} for a thicker HAGFF electrode (200 μm), probably due to the increased difficulty for ion transport. Besides, overlaying several layers of textile electrodes is known as a simple way to prepare thicker electrodes. We stacked two layers 200 μm HAGFF into a single electrode and reached a capacitance of 3122 mF cm^{-2}, better than the highest value of ever reported carbon fiber cloth-based electrodes with equivalent thickness (0.4–0.5 mm).[23] More surprisingly, five layers of HAGFF electrodes could even

DOI: 10.1021/acsnano.7b05092
ACS Nano XXXX, XXX, XXX–XXX

achieve 7398 mF cm^{-2}, but its rate performance is largely degraded at the same time. Although thicker electrodes endow the supercapacitors with higher areal capacitance and energy density,[52] the power density is obviously decreased,[23,49] not to mention the loss of flexibility. Thus, we believe that thinner electrodes with sufficient capacitance, and good rate capability, as well as being lightweight, are more suitable for practical wearable devices. Given this consideration, HAGFF electrodes of modest thickness (~150 μm, with the highest C_G of 244 F g^{-1} and C_A of 1060 mF cm^{-2}) are regarded as the optimal ones in our study.

The high flexibility and good structural stability of HAGFFs ensure their application as electrodes in wearable supercapacitors. As a prototype for demonstration, we assembled two pieces of HAGFFs symmetrically into an all-solid-state supercapacitor using poly(vinyl alcohol) (PVA)/H_2SO_4 gel as the solid electrolyte and separator (Figure 8a). The areal capacitance and the maximum energy density are shown to be better than the results obtained by others[10,12] (Figure S9), due to the enhanced electrochemical performance of HAGFFs. Figure 8 panels b and c show that the solid-state supercapacitor is easily bent to 180° without breaking, and the CV curves are barely changed while bending and releasing. After bending for 300 cycles, the HAGFF electrode exhibits 92.2% capacitance retention (Figure 8d), indicating a stable capacitive performance through deformation.

CONCLUSION

We reported the fabrication of hierarchical graphene fibers and GFFs *via* a hydrothermal activation process. Such a protocol, based on the crumpling of graphene sheets, is simple, controllable, efficient, and particularly suitable for GO-based materials. We believe it is able to be extended as a general activation strategy for various as-formed GO assemblies. The HAGFFs with largely increased surface area displayed the highest areal capacitance compared to other carbon textile electrodes, including carbon fiber cloths. Given that carbon fiber cloths are very popular as electrodes in certain functional devices, our HAGFFs with distinct superiorities may have a bright prospect in such a hot field. The hierarchical feature may allow the use of HAGFFs in many applications, which should not be limited to the electrodes for supercapacitors, but also for batteries, fuel cells, water splitting systems, *etc.* Moreover, conventional modifying methods for higher electrochemical performance, such as doping strategy and incorporation of active materials, are also applicable to our HAGFFs, providing a possible path to high-performance textile electrodes.

METHODS

Preparation of Graphene Oxide Fiber Fabrics. Continuous GO fibers were spun *via* injecting GO/DMF solution (~5 mg mL^{-1}, purchased from Hangzhou Gaoxi Technology Co., Ltd.) into a coagulation bath of ethyl acetate and collected on a spool, according to previous reports.[53,54] After being dried at room temperature overnight and then 100 °C for 3 h under vacuum, the GO fibers were immersed in ethanol and chopped into short fibers using a high-speed shearing machine. Then the GO short fibers were deposited on a plastic mesh and dried at 80 °C for 10 h. Finally, the plastic mesh was removed to get the free-standing nonwoven GOFFs.

Preparation of Hydrothermally Activated Graphene Fiber Fabrics. The as-spun GO fibers were dried at room temperature overnight and another 3 h at 60 °C under vacuum. Then the fibers were put in a sealed autoclave containing deionized water and heated at 150 °C for 10 h. After the hydrothermal treatment, the partially reduced gel fibers were cut into short fibers using a high-speed shearing machine and collected on a plastic mesh. The wet cake of graphene fibers was dried in air at room temperature for at least 24 h and the free-standing HAGFFs were obtained after the plastic mesh was taken off.

Assembly of All-Solid-State Supercapacitors. The PVA/H_2SO_4 gel electrolyte was prepared by adding 4 g PVA (average molecular weight: 88000) in 40 mL of 1 M H_2SO_4 solution at 85 °C *via* continuous stirring until the PVA was completely dissolved. Two identical pieces of HAGFF were soaked in the gel electrolyte for 5 min to allow the penetration of electrolyte into their network structure. After being dried separately, the two pieces of HAGFF were stacked together with a drop of gel electrolyte in between and dried at room temperature to obtain the symmetrical all-solid-state supercapacitor.

Characterization. SEM images were taken on a Hitachi S4800 field-emission SEM system. TEM images were collected on a transmission electron microscope (Tecnai G2 F20 S-TWIN). XPS was performed using a PHI 5000C ESCA system operated at 14.0 kV. XRD measurements were taken on a Philips X'Pert PRO diffractometer using Cu Kα radiation (λ = 1.5418 Å). Raman spectra were acquired using a Renishaw inVia-Reflex Raman microscopy at an excitation wavelength of 532 nm.

Electrochemical Characterization. Before electrochemical characterization, the as-prepared GOFFs and HAGFFs were chemically reduced by hydrazine hydrate at 95 °C for 10 h. Electrochemical performance of the obtained GFF and HAGFF electrodes were tested on an electrochemical workstation (CHI 660e, CH Instruments, Inc.) with two symmetrical electrodes, using a mixed cellulose esters membrane as separator (pore size 0.22 μm), and 1 M H_2SO_4 aqueous solution as electrolyte. The effective area of each textile electrode was ~0.8 cm^2. The cycling performance was tested by GCD sweeps at a scan rate of 1 A g^{-1} for 50000 cycles. EIS test was performed under open-circuit potential from a frequency of 100 kHz to 10 mHz.

Calculation of the Electrochemical Performance. Specific areal capacitance (C_A) of GFF electrodes were calculated from their GCD curves according to the equation: $C_A = 2 \times I \times t \times U^{-1} \times S^{-1}$, where I stands for charge−discharge current, t is the discharge time, U is the potential window, and S is the area of a single electrode. Gravimetric capacitance (C_G) was derived from the equation: $C_A = 2 \times I \times t \times U^{-1} \times M^{-1}$, where M is the mass of a single electrode. The areal energy density (E_A) and areal power density (P_A) of the assembled supercapacitors were obtained from $E_A = 0.125 \times C_A \times U^2$ and $P_A = E_A \times t^{-1}$, respectively.

ASSOCIATED CONTENT

Supporting Information

The Supporting Information is available free of charge on the ACS Publications website at DOI: 10.1021/acsnano.7b05092.

Additional information for the comparison between GOFF and HAGFF, the optimization of hydrothermal activation, and further characterization on the electrochemical performance of the textile electrodes (PDF)

AUTHOR INFORMATION

Corresponding Authors

*E-mail: wwgao@zju.edu.cn.

*E-mail: chaogao@zju.edu.cn.

ORCID

Zhen Xu: 0000-0001-9282-9753

Chao Gao: 0000-0002-3893-7224

Notes

The authors declare no competing financial interest.

ACKNOWLEDGMENTS

This work was supported by the National Natural Science Foundation of China (Nos. 21325417, 51603183, and

DOI: 10.1021/acsnano.7b05092
ACS Nano XXXX, XXX, XXX−XXX

51533008), National Key R&D Program of China (No. 2016YFA0200200), Fundamental Research Funds for the Central Universities (Nos. 2017XZZX008-06 and 2017QNA4036), and the Hundred Talents Program of Zhejiang University (188020*194231701/113).

REFERENCES

(1) He, Y.; Chen, W.; Gao, C.; Zhou, J.; Li, X.; Xie, E. An Overview of Carbon Materials for Flexible Electrochemical Capacitors. *Nanoscale* **2013**, *5*, 8799−8820.
(2) Dong, L.; Xu, C.; Li, Y.; Huang, Z.-H.; Kang, F.; Yang, Q.-H.; Zhao, X. Flexible Electrodes and Supercapacitors for Wearable Energy Storage: A Review by Category. *J. Mater. Chem. A* **2016**, *4*, 4659−4685.
(3) Gulzar, U.; Goriparti, S.; Miele, E.; Li, T.; Maidecchi, G.; Toma, A.; De Angelis, F.; Capiglia, C.; Zaccaria, R. P. Next-Generation Textiles: From Embedded Supercapacitors to Lithium Ion Batteries. *J. Mater. Chem. A* **2016**, *4*, 16771−16800.
(4) Simon, P.; Gogotsi, Y. Materials for Electrochemical Capacitors. *Nat. Mater.* **2008**, *7*, 845−854.
(5) Wang, Y.; Shi, Z.; Huang, Y.; Ma, Y.; Wang, C.; Chen, M.; Chen, Y. Supercapacitor Devices Based on Graphene Materials. *J. Phys. Chem. C* **2009**, *113*, 13103−13107.
(6) Béguin, F.; Presser, V.; Balducci, A.; Frackowiak, E. Carbons and Electrolytes for Advanced Supercapacitors. *Adv. Mater.* **2014**, *26*, 2219−2251.
(7) Wang, X.; Lu, X.; Liu, B.; Chen, D.; Tong, Y.; Shen, G. Flexible Energy-Storage Devices: Design Consideration and Recent Progress. *Adv. Mater.* **2014**, *26*, 4763−4782.
(8) Liu, W.; Song, M.-S.; Kong, B.; Cui, Y. Flexible and Stretchable Energy Storage: Recent Advances and Future Perspectives. *Adv. Mater.* **2017**, *29*, 1603436.
(9) Liu, L.; Niu, Z.; Zhang, L.; Zhou, W.; Chen, X.; Xie, S. Nanostructured Graphene Composite Papers for Highly Flexible and Foldable Supercapacitors. *Adv. Mater.* **2014**, *26*, 4855−4862.
(10) Dong, L.; Xu, C.; Li, Y.; Pan, Z.; Liang, G.; Zhou, E.; Kang, F.; Yang, Q.-H. Breathable and Wearable Energy Storage Based on Highly Flexible Paper Electrodes. *Adv. Mater.* **2016**, *28*, 9313−9319.
(11) Weng, Z.; Su, Y.; Wang, D.-W.; Li, F.; Du, J.; Cheng, H.-M. Graphene-Cellulose Paper Flexible Supercapacitors. *Adv. Energy Mater.* **2011**, *1*, 917−922.
(12) Sun, H.; Xie, S.; Li, Y.; Jiang, Y.; Sun, X.; Wang, B.; Peng, H. Large-Area Supercapacitor Textiles with Novel Hierarchical Conducting Structures. *Adv. Mater.* **2016**, *28*, 8431−8438.
(13) Hu, L.; Chen, W.; Xie, X.; Liu, N.; Yang, Y.; Wu, H.; Yao, Y.; Pasta, M.; Alshareef, H. N.; Cui, Y. Symmetrical MnO_2-Carbon Nanotube-Textile Nanostructures for Wearable Pseudocapacitors with High Mass Loading. *ACS Nano* **2011**, *5*, 8904−8913.
(14) Hu, L.; Pasta, M.; La Mantia, F.; Cui, L.; Jeong, S.; Deshazer, H. D.; Choi, J. W.; Han, S. M.; Cui, Y. Stretchable, Porous, and Conductive Energy Textiles. *Nano Lett.* **2010**, *10*, 708−714.
(15) Liang, Q.; Ye, L.; Xu, Q.; Huang, Z.-H.; Kang, F.; Yang, Q.-H. Graphitic Carbon Ntride Nanosheet-Assisted Preparation of N-Enriched Mesoporous Carbon Nanofibers with Improved Capacitive Performance. *Carbon* **2015**, *94*, 342−348.
(16) Li, L.; Zhong, Q.; Kim, N. D.; Ruan, G.; Yang, Y.; Gao, C.; Fei, H.; Li, Y.; Ji, Y.; Tour, J. M. Nitrogen-Doped Carbonized Cotton for Highly Flexible Supercapacitors. *Carbon* **2016**, *105*, 260−267.
(17) Xue, J.; Zhao, Y.; Cheng, H.; Hu, C.; Hu, Y.; Meng, Y.; Shao, H.; Zhang, Z.; Qu, L. An All-Cotton-Derived, Arbitrarily Foldable, High-Rate, Electrochemical Supercapacitor. *Phys. Chem. Chem. Phys.* **2013**, *15*, 8042−8045.
(18) Wang, J.; Tang, J.; Xu, Y.; Ding, B.; Chang, Z.; Wang, Y.; Hao, X.; Dou, H.; Kim, J. H.; Zhang, X.; Yamauchi, Y. Interface Miscibility Induced Double-Capillary Carbon Nanofibers for Flexible Electric Double Layer Capacitors. *Nano Energy* **2016**, *28*, 232−240.
(19) Lam, D. V.; Jo, K.; Kim, C.-H.; Kim, J.-H.; Lee, H.-J.; Lee, S.-M. Activated Carbon Textile *via* Chemistry of Metal Extraction for Supercapacitors. *ACS Nano* **2016**, *10*, 11351−11359.
(20) Ke, Q.; Guan, C.; Zhang, X.; Zheng, M.; Zhang, Y. W.; Cai, Y.; Zhang, H.; Wang, J. Surface-Charge-Mediated Formation of H-TiO_2@$Ni(OH)_2$ Heterostructures for High-Performance Supercapacitors. *Adv. Mater.* **2017**, *29*, 1604164.
(21) Wang, G.; Wang, H.; Lu, X.; Ling, Y.; Yu, M.; Zhai, T.; Tong, Y.; Li, Y. Solid-State Supercapacitor Based on Activated Carbon Cloths Exhibits Excellent Rate Capability. *Adv. Mater.* **2014**, *26*, 2676−2682.
(22) Wang, W.; Liu, W.; Zeng, Y.; Han, Y.; Yu, M.; Lu, X.; Tong, Y. A Novel Exfoliation Strategy to Significantly Boost the Energy Storage Capability of Commercial Carbon Cloth. *Adv. Mater.* **2015**, *27*, 3572−3578.
(23) Dong, L.; Xu, C.; Li, Y.; Wu, C.; Jiang, B.; Yang, Q.; Zhou, E.; Kang, F.; Yang, Q.-H. Simultaneous Production of High-Performance Flexible Textile Electrodes and Fiber Electrodes for Wearable Energy Storage. *Adv. Mater.* **2016**, *28*, 1675−1681.
(24) Li, Z.; Xu, Z.; Liu, Y.; Wang, R.; Gao, C. Multifunctional Non-Woven Fabrics of Interfused Graphene Fibres. *Nat. Commun.* **2016**, *7*, 13684.
(25) Liu, Y.; Xu, Z.; Gao, W.; Cheng, Z.; Gao, C. Graphene and Other 2D Colloids: Liquid Crystals and Macroscopic Fibers. *Adv. Mater.* **2017**, *29*, 1606794.
(26) Cheng, H.; Dong, Z.; Hu, C.; Zhao, Y.; Hu, Y.; Qu, L.; Chen, N.; Dai, L. Textile Electrodes Woven by Carbon Nanotube-Graphene Hybrid Fibers for Flexible Electrochemical Capacitors. *Nanoscale* **2013**, *5*, 3428−3434.
(27) Meng, F.; Lu, W.; Li, Q.; Byun, J.-H.; Oh, Y.; Chou, T.-W. Graphene-Based Fibers: A Review. *Adv. Mater.* **2015**, *27*, 5113−5131.
(28) Kou, L.; Huang, T.; Zheng, B.; Han, Y.; Zhao, X.; Gopalsamy, K.; Sun, H.; Gao, C. Coaxial Wet-Spun Yarn Supercapacitors for High-Energy Density and Safe Wearable Electronics. *Nat. Commun.* **2014**, *5*, 3754.
(29) Cheng, H.; Hu, C.; Zhao, Y.; Qu, L. Graphene Fiber: A New Material Platform for Unique Applications. *NPG Asia Mater.* **2014**, *6*, e113.
(30) Meng, Y.; Zhao, Y.; Hu, C.; Cheng, H.; Hu, Y.; Zhang, Z.; Shi, G.; Qu, L. All-Graphene Core-Sheath Microfibers for All-Solid-State, Stretchable Fibriform Supercapacitors and Wearable Electronic Textiles. *Adv. Mater.* **2013**, *25*, 2326−2331.
(31) Li, Z.; Liu, Z.; Sun, H.; Gao, C. Superstructured Assembly of Nanocarbons: Fullerenes, Nanotubes, and Graphene. *Chem. Rev.* **2015**, *115*, 7046−117.
(32) Wang, J.; Kaskel, S. KOH Activation of Carbon-Based Materials for Energy Storage. *J. Mater. Chem.* **2012**, *22*, 23710−23725.
(33) Xu, Z.; Gao, C. Graphene Chiral Liquid Crystals and Macroscopic Assembled Fibres. *Nat. Commun.* **2011**, *2*, 571.
(34) Xu, Z.; Gao, C. Graphene in Macroscopic Order: Liquid Crystals and Wet-Spun Fibers. *Acc. Chem. Res.* **2014**, *47*, 1267−1276.
(35) Dong, Z.; Jiang, C.; Cheng, H.; Zhao, Y.; Shi, G.; Jiang, L.; Qu, L. Facile Fabrication of Light, Flexible and Multifunctional Graphene Fibers. *Adv. Mater.* **2012**, *24*, 1856−1861.
(36) Zhou, Y.; Bao, Q.; Tang, L. A. L.; Zhong, Y.; Loh, K. P. Hydrothermal Dehydration for the "Green" Reduction of Exfoliated Graphene Oxide to Graphene and Demonstration of Tunable Optical Limiting Properties. *Chem. Mater.* **2009**, *21*, 2950−2956.
(37) Xu, Y.; Sheng, K.; Li, C.; Shi, G. Self-Assembled Graphene Hydrogel *via* a One-Step Hydrothermal Process. *ACS Nano* **2010**, *4*, 4324−4330.
(38) Zhang, L.; Shi, G. Preparation of Highly Conductive Graphene Hydrogels for Fabricating Supercapacitors with High Rate Capability. *J. Phys. Chem. C* **2011**, *115*, 17206−17212.
(39) Wu, K.-H.; Wang, D.-W.; Gentle, I. R. Revisiting Oxygen Reduction Reaction on Oxidized and Unzipped Carbon Nanotubes. *Carbon* **2015**, *81*, 295−304.
(40) Zhang, J.; Lv, W.; Tao, Y.; He, Y.-B.; Wang, D.-W.; You, C.-H.; Li, B.; Kang, F.; Yang, Q.-H. Ultrafast High-Volumetric Sodium

DOI: 10.1021/acsnano.7b05092
ACS Nano XXXX, XXX, XXX−XXX

Storage of Folded-Graphene Electrodes Through Surface-Induced Redox Reactions. *Energy Stor. Mater.* **2015**, *1*, 112−118.
(41) Bi, H.; Yin, K.; Xie, X.; Zhou, Y.; Wan, N.; Xu, F.; Banhart, F.; Sun, L.; Ruoff, R. S. Low Temperature Casting of Graphene with High Compressive Strength. *Adv. Mater.* **2012**, *24*, 5124−5129.
(42) Bosch-Navarro, C.; Coronado, E.; Marti-Gastaldo, C.; Sanchez-Royo, J. F.; Gomez, M. G. Influence of the pH on the Synthesis of Reduced Graphene Oxide under Hydrothermal Conditions. *Nanoscale* **2012**, *4*, 3977−3982.
(43) Zhang, F.; Liu, T.; Li, M.; Yu, M.; Luo, Y.; Tong, Y.; Li, Y. Multiscale Pore Network Boosts Capacitance of Carbon Electrodes for Ultrafast Charging. *Nano Lett.* **2017**, *17*, 3097−3104.
(44) Zhao, J.; Lai, H.; Lyu, Z.; Jiang, Y.; Xie, K.; Wang, X.; Wu, Q.; Yang, L.; Jin, Z.; Ma, Y.; Liu, J.; Hu, Z. Hydrophilic Hierarchical Nitrogen-Doped Carbon Nanocages for Ultrahigh Supercapacitive Performance. *Adv. Mater.* **2015**, *27*, 3541−3545.
(45) Worsley, M. A.; Charnvanichborikarn, S.; Montalvo, E.; Shin, S. J.; Tylski, E. D.; Lewicki, J. P.; Nelson, A. J.; Satcher, J. H.; Biener, J.; Baumann, T. F.; Kucheyev, S. O. Toward Macroscale, Isotropic Carbons with Graphene-Sheet-Like Electrical and Mechanical Properties. *Adv. Funct. Mater.* **2014**, *24*, 4259−4264.
(46) Tao, Y.; Xie, X.; Lv, W.; Tang, D.-M.; Kong, D.; Huang, Z.; Nishihara, H.; Ishii, T.; Li, B.; Golberg, D.; Kang, F.; Kyotani, T.; Yang, Q.-H. Towards Ultrahigh Volumetric Capacitance: Graphene Derived Highly Dense but Porous Carbons for Supercapacitors. *Sci. Rep.* **2013**, *3*, 2975.
(47) Zhang, C.; Liu, D.-H.; Lv, W.; Wang, D.-W.; Wei, W.; Zhou, G.-M.; Wang, S.; Li, F.; Li, B.-H.; Kang, F.; Yang, Q.-H. A High-Density Graphene-Sulfur Assembly: A Promising Cathode for Compact Li-S batteries. *Nanoscale* **2015**, *7*, 5592−5597.
(48) Qiu, L.; Zhang, X.; Yang, W.; Wang, Y.; Simon, G. P.; Li, D. Controllable Corrugation of Chemically Converted Graphene Sheets in Water and Potential Application for Nanofiltration. *Chem. Commun.* **2011**, *47*, 5810−5812.
(49) Dong, L.; Xu, C.; Yang, Q.; Fang, J.; Li, Y.; Kang, F. High-Performance Compressible Supercapacitors Based on Functionally Synergic Multiscale Carbon Composite Textiles. *J. Mater. Chem. A* **2015**, *3*, 4729−4737.
(50) Zhao, J.; Jiang, Y.; Fan, H.; Liu, M.; Zhuo, O.; Wang, X.; Wu, Q.; Yang, L.; Ma, Y.; Hu, Z. Porous 3D Few-Layer Graphene-like Carbon for Ultrahigh-Power Supercapacitors with Well-Defined Structure-Performance Relationship. *Adv. Mater.* **2017**, *29*, 1604569.
(51) Xu, B.; Yue, S.; Sui, Z.; Zhang, X.; Hou, S.; Cao, G.; Yang, Y. What is the Choice for Supercapacitors: Graphene or Graphene Oxide? *Energy Environ. Sci.* **2011**, *4*, 2826−2830.
(52) Stoller, M. D.; Park, S.; Zhu, Y.; An, J.; Ruoff, R. S. Graphene-Based Ultracapacitors. *Nano Lett.* **2008**, *8*, 3498−3502.
(53) Liu, Y.; Xu, Z.; Zhan, J.; Li, P.; Gao, C. Superb Electrically Conductive Graphene Fibers *via* Doping Strategy. *Adv. Mater.* **2016**, *28*, 7941−7947.
(54) Xu, Z.; Liu, Y.; Zhao, X.; Peng, L.; Sun, H.; Xu, Y.; Ren, X.; Jin, C.; Xu, P.; Wang, M.; Gao, C. Ultrastiff and Strong Graphene Fibers *via* Full-Scale Synergetic Defect Engineering. *Adv. Mater.* **2016**, *28*, 6449−6456.

DOI: 10.1021/acsnano.7b05092
ACS Nano XXXX, XXX, XXX−XXX